Inorganic Chemistry
Article

Inorg. Chem. **2009**, *48*, 5663–5676 **5663**
DOI: 10.1021/ic801295c

Microcrystalline Hexagonal Tungsten Bronze. 2. Dehydration Dynamics

Vittorio Luca,*,§ Christopher S. Griffith, and John V. Hanna#

Australian Nuclear Science and Technology Organisation, ANSTO Minerals, New Illawarra Road, Lucas Heights, NSW 2234, Australia. § Present address: Comisión Nacional de Energía Atómica, Centro Atómico Constituyentes, Av. General Paz 1499,1650 San Martin, Provincia de Buenos Aires, Argentina. # Present address: Department of Physics, University of Warwick, Gibbet Hill Rd., Coventry CV4 7AL, United Kingdom.

Received July 10, 2008

Low-temperature (25−600 °C) thermal transformations have been studied for hydrothermally prepared, microcrystalline hexagonal tungsten bronze (HTB) phases $A_xWO_{3+x/2}\cdot zH_2O$ as a function of temperature, where A is an exchangeable cation (in this case Na^+ or Cs^+) located in hexagonal structural tunnels. Thermal treatment of the as-prepared sodium- and cesium-exchanged phases in air were monitored using a conventional laboratory-based X-ray diffractometer, while thermal transformations in vacuum were studied using synchrotron X-ray and neutron diffraction. Concurrent thermogravimetric, diffuse reflectance infrared (DRIFT), and ^{23}Na and ^{133}Cs magic angle spinning (MAS) NMR spectroscopic studies have also been undertaken. For the cesium variant, cell volume contraction occurred from room temperature to about 350 °C, the regime in which water was "squeezed" out of tunnel sites. This was followed by a lattice expansion in the 350−600 °C temperature range. Over the entire temperature range, a net thermal contraction was observed, and this was the result of an anisotropic change in the cell dimensions which included a shortening of the A−O2 bond length. These changes explain why Cs^+ ions are locked into tunnel positions at temperatures as low as 400 °C, subsequently inducing a significant reduction in Cs^+ extractability under low pH (nitric acid) conditions. The changing Cs^+ speciation as detected by ^{133}Cs MAS NMR showed a condensation from multiple Cs sites, presumably associated with differing modes of Cs^+ hydration in the tunnels, to a single Cs^+ environment upon thermal transformation and water removal. While similar lattice contraction was observed for the as-prepared sodium variant, the smaller radius of Na^+ caused it to be relatively easily removed with acid in comparison to the Cs^+ variant. From ^{23}Na MAS NMR studies of the parent material, complex Na^+ speciation was observed with dehydrated and various hydrated Na^+ species being identified, and a subsequent dynamic interchange within this speciation was observed upon thermal treatment.

1. Introduction

Tungsten oxides have been extensively studied in recent years, especially in the context of their chromogenic properties.[1] Tungsten oxides with the hexagonal tungsten bronze (HTB) structure (Figure 1) were first prepared more than five decades ago. Magneli described the structure of the reduced A_xWO_3 (A = K, Rb, and Cs) HTBs, which were prepared by heating mixtures of WO_3 with K, Rb, or Cs tungstates in reducing atmospheres.[2] Other HTB phases with the nominal formula, A_xWO_3, have also been traditionally prepared using high-temperature methods in reducing environments. For such reduced compounds, the charge compensation is due to pentavalent tungsten atoms, and therefore the general formula should be written as $A_xW^{(6-x)+}O_3$. In these cases, the type of structure that is formed is dependent on the identity of the cation that occupies the tunnel positions and the stoichiometry. Large tunnel cations (e.g., Rb^+, Cs^+) generally favor the formation of hexagonal structures, as depicted in Figure 1. It is also possible that a single tunnel cation can give rise to different structures depending on the value of x in the formula. These reduced bronze compounds typically show a positive thermal expansion as the temperature increases.[3]

Gerand et al.[4] were the first to synthesize hydrous tungsten trioxide compounds with a hexagonal tungsten bronze-like structure (Figure 1) through wet chemical methods. The compound they synthesized also possessed hexagonal tunnels and a very similar structure to the classical reduced HTB phase but with orthorhombic symmetry and structural water molecules, as indicated by the formula

*To whom correspondence should be addressed. Phone: 54-11-6772 7018. E-mail: vluca@cnea.gov.ar.

(1) Bange, K. *Sol. Energy Mater. Sol. Cells* **1999**, *58*, 1.
(2) Magneli, A. *Acta Chem. Scand.* **1953**, *7*, 315.
(3) Werner, P. E.; Kierkegaard, P.; Magneli, A. *Acta Chem. Scand.* **1961**, *15*, 427.
(4) Gerand, B.; Nowogrocki, G.; Guenot, J.; Figlarz, M. *J. Solid State Chem.* **1979**, *29*, 429.

© 2009 American Chemical Society
Published on Web 06/11/2009

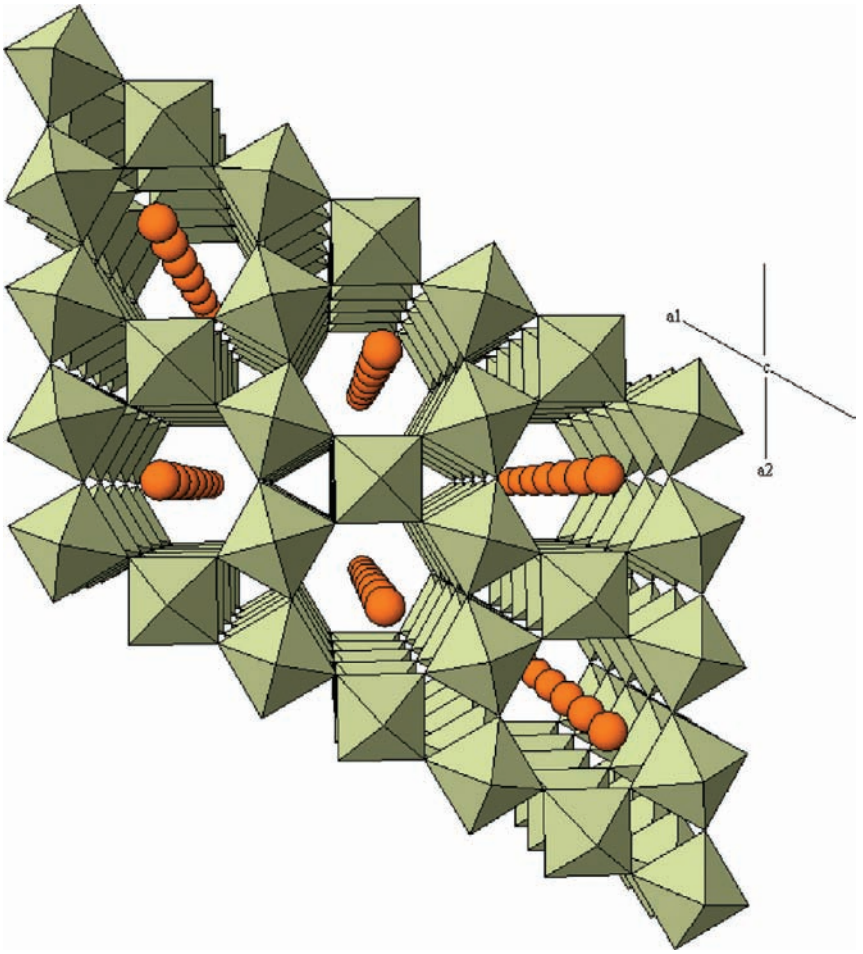

Figure 1. Polyhedral representation of the HTB structure viewed down the *c* axis. The A cations (Cs^+ and Na^+) are portrayed as spheres.

given as $WO_3 \cdot {}^1/_3H_2O$. Related compounds were later described by Figlarz,[5] who also discussed thermally driven structural transformations in empty-tunnel orthorhombic $Mo_xW_{1-x}O_3$ compounds. The hexagonal-type orthorhombic $WO_3 \cdot {}^1/_3H_2O$ exhibited thermal stability to about 300 °C, after which it converted to a supermetastable hexagonal WO_3 compound, and then, at about 500 °C, to thermodynamically stable monoclinic WO_3.[6] These transformations are classed as reconstructive, as there is a change in the secondary coordination of the WO_6 polyhedra without any change in primary coordination; that is, bonds must be broken. It is presumably the water present in the hexagonal tunnels that stabilizes the initially hydrated orthorhombic structure.

Kudo et al.[7] were the first to describe the preparation of HTB phases from peroxo-polytungstate solutions. Distinct phases were obtained depending on the atmosphere used for the thermal decomposition of the peroxo-polytungstate precursor. Heating in oxidizing atmosphere gave rise to phases with the formula $M_xWO_{3+x/2}$ or $M_xW_{1+x/6}O_3$, depending on whether charge compensation was achieved through the inclusion in the structure of excess oxygen or via tungsten vacancies.[8]

The synthesis of hexagonal pyrochlore and perovskite tungsten oxides containing Na^+ cations in tunnel sites can be achieved by adjusting the pH of a sodium tungstate solution followed by hydrothermal treatment at low temperatures (140−200 °C), as first demonstrated by Reis and co-workers.[9,10]

These hydrated microcrystalline materials have a pale yellow-green coloration, and therefore the tungsten is predominantly hexavalent. The charge compensation mechanism in these systems is presumed to be due to oxygen atoms present in the tunnel sites, and therefore the formula may be given as $A_xWO_{3+x/2} \cdot zH_2O$.

The structure of these HTB phases, where $A = Na^+$, have been analyzed using Rietveld techniques.[11] The structure was refined in space group *P*6/*mmm* and was reported to be similar to that of high-temperature reduced HTB, only that it contained Na^+ ions at (0, 0, 0) together with water molecules along the hexagonal tunnel with the water oxygen positioned at (0, 0, 0.4) (Table 1). In addition to water molecules, oxygen anions and hydroxyl groups may also be present in these tunnel positions. These oxygen atoms that are present in tunnel sites are presumed to diffuse in and out of the tunnels as the material is oxidized and reduced.

(5) Figlarz, M. *Prog. Solid State Chem.* **1989**, *19*, 1.
(6) Seguin, L.; Figlarz, M.; Cavagnat, R.; Lassegues, J.-C. *Spectrochim. Acta, Part A* **1995**, *51A*, 1323.
(7) Kudo, T.; Kishimoto, A.; Oi, J.; Inoue, H. *Solid State Ionics* **1990**, *40*−*41*, 567.
(8) Tsuyumoto, I.; Kishimoto, A.; Kudo, T. *Solid State Ionics* **1993**, *59*, 211.
(9) Reis, K. P.; Ramanan, A.; Whittingham, M. S. *Chem. Mater.* **1990**, *2*, 219.
(10) Reis, K. P.; Ramanan, A.; Whittingham, M. S. *J. Solid State Chem.* **1992**, *96*, 31.
(11) Reis, K. P.; Prince, E.; Whittingham, M. S. *Chem. Mater.* **1992**, *4*, 307.

Table 1. Typical Unit Cell Parameters for As-Prepared Na−W−HTB

	x	*y*	*z*
W	1/2	0	1/2
O1	1/2	0	0
O2	0.2114	2*x*	0
O3(W)	0	0	0.415
Na	0	0	0

It has long been realized that some of the tunnel Na^+ cations are relatively easily replaced by other alkali metal cations including K^+, Cs^+, alkaline earth cations, and trivalent cations. What has not been generally appreciated is the fact that the tunnel dimensions confer on these phases a particularly high selectivity for cations with ionic radii around 1.2 and 1.7 Å, making them selective for Cs^+ and Sr^{2+} and therefore potentially useful for the pretreatment of radioactive wastes containing $^{137}Cs^+$ and $^{90}Sr^{2+}$.[12,13] In addition to selectivity for Cs^+ and Sr^{2+}, these materials display a particularly high selectivity for Ag^+ and radiogenic $^{210}Pb^{2+}$ and $^{210}Po^{4+}$.[14] We have found recently that both Cs^+ and Sr^{2+} can be sorbed by these materials from even strongly acidic solutions in which they are extremely stable. Moreover, once these cations have been extracted from solution, it is possible to immobilize the cations within the structure of the bronzoid phase by simply heating it in the air to temperatures in the range 600−1300 °C.[15−17] The resultant multicomponent phase assemblages were highly leach-resistant and performed at least as well as any of the more traditionally studied waste form materials such as titanate ceramics, vitrified glasses, and composite glass ceramic formulations using either PCT-B or MCC-1 testing protocols.

In a companion publication in this issue (part 1), we reported a detailed study of the cation siting in these hydrous HTB compounds aimed at elucidating the basis of their cation selectivity. As in well-known and studied microporous materials, physical properties change with subtle structural changes during relatively mild dehydration. The aim of the present study was therefore to provide a detailed structural understanding of dehydration processes or dehydration dynamics of the Na^+− and Cs^+−containing HTB phases and to inquire as to how tunnel dimensions change in response to dehydration. In addition, we were also seeking to shed light on how these thermal transformations varied with different tunnel cations, in particular Na^+ and Cs^+.

2. Experimental Section

The sample of $Na_xWO_{3+x/2}\cdot zH_2O$ (Na−W−HTB) was synthesized by previously published methods[9] which involved reducing the pH of a 1.0 M sodium tungstate solution to 1.72 using 1 M HCl followed by hydrothermal treatment of the resulting pale yellow solution in a Teflon-lined stainless steel autoclave at 155 °C. After five days of reaction, the pale yellow-green powder was separated by vacuum filtration, washed extensively with deionized water, and dried in an oven at 75 °C.

Preparation of the cesium-exchanged variant (Cs−W−HTB) was carried out by contacting a given mass of Na−W−HTB with a 1 M HNO_3 solution containing a calculated amount of Cs^+ necessary to achieve exchange of a certain amount of the tunnel sodium cations.[13] The level of Cs^+ exchange was determined by measuring the amount of Cs^+ removed from solution using Inductively Coupled Plasma Mass Spectrometry (ICP-MS). The composition of the Cs−W−HTB phase examined was nominally $A_{0.15}Cs_{0.05}WO_3\cdot zH_2O$, where A in this case was a mixture of Na^+ initially present in the tunnels, which cannot be extracted, and H^+, which was introduced during the ion exchange in 1 M HNO_3 (see part 1).

X-ray diffraction (XRD) patterns of the Na− and Cs−W−HTB phases which had been thermally treated in the air at given temperatures were carried out on a Scintag X1 diffractometer using Cu Kα radiation and a Peltier cooled detector. Samples were prepared by heating them in air at given temperatures and then they were packed into conventional rectangular holders for the recording of diffraction patterns.

Dynamic heating experiments were carried out in situ using synchrotron radiation on Beamline 20B at the Australian National Beamline Facility at the Photon Factory, Tsukuba, Japan. The X-ray diffractometer employed the Debye−Scherrer geometry with a 573 mm radius, and the data were recorded onto three Fuji image plates.[18] The X-ray wavelength was calibrated using Si (NBS-640) and was found to be 1.2499 Å. Finely ground samples were packed into 0.30 mm quartz capillaries, which were either flame-sealed or left open at one end, depending on whether samples were to be heated in vacuum or in an atmosphere of humid air, respectively. Image plate data were taken at 25 °C intervals typically starting from 25 °C. The capillary sample was heated in a home-built tubular furnace, in which a thermocouple was located as close to the sample end of the capillary as possible. A ramp-and-pause mode was chosen for the heating runs and consisted of a 10 °C per minute ramp, a 5 min hold, and a 10 min exposure time to record the pattern.

The X-ray powder diffraction data were refined using the Rietveld program Rietica.[19,20] The structural parameters in Table 1 were used for the initial refinement. The background for each pattern was fit by selecting points and fitting a cubic spline function through the selected points. Usually, good fits were achieved, but occasionally, negative isotropic thermal parameters were obtained for some of the atoms. In these cases, the isotropic thermal parameters were constrained during the initial stages of the refinement and only freed toward the end of the process. However, the most important structural information required from these refinements was the unit cell parameters, which could be derived extremely precisely and accurately using powder diffraction experiments and the Rietveld method.

Bulk elemental analysis of the as-prepared water-washed Na−W−HTB phase dried at 70 °C typically gave Na/W ratios of 1.1, as measured by X-ray fluorescence spectroscopy. Energy dispersive spectroscopy (EDS) analysis of individual fibers from acid-washed samples using transmission electron microscopy routinely showed Na/W ratios of 0.2 (Figure 2). This confirmed that the as-prepared water-washed Na−W−HTB phase contained excess sodium not

(12) Luca, V.; Griffith, C. S.; Chronis, H.; Widjaja, J.; Li, H.; Scales, N. *Mater. Res. Soc. Symp. Proc.* **2004**, *807*, 309.
(13) Griffith, C. S.; Luca, V. *Chem. Mater.* **2004**, *16*, 4992.
(14) Secomb, R. J.; Griffith, C. S.; Brown, S. A.; Luca, V. *Radiochim. Acta* **2007**, *95*, 1.
(15) Griffith, C. S.; Sebesta, F.; Hanna, J. V.; Yee, P.; Drabarek, E.; Smith, M. E.; Luca, V. *J. Nucl. Mater.* **2006**, *358*, 151.
(16) Luca, V.; Griffith, C. S.; Drabarek, E.; Chronis, H. *J. Nucl. Mater.* **2006**, *358*, 139.
(17) Luca, V.; Drabarek, E.; Chronis, H.; Mcleod, T. *J. Nucl. Mater.* **2006**, *358*, 164.
(18) Sabine, T. M.; Kennedy, B. J.; Garrett, R. F.; Foran, G. J.; Cookson, D. J. *J. Appl. Crystallogr.* **1995**, *28*, 513.
(19) Hill, R. J.; Howard, C. J.; Hunter B. A. *Computer Program for Rietveld Analysis of Fixed Wavelength X-Ray and Neutron Powder Diffraction Patterns*; Australian Atomic Energy Commission (Now ANSTO), Rept. No. M112, Lucas Heights Research Laboratories: New South Wales, Australia, **1995**. Available at www.Rietica.Org (accessed Apr 2009).
(20) Hunter, B. A. *International Union of Crystallography, Commission on Powder Diffraction Newsletter* **1998**, *20*, 21.

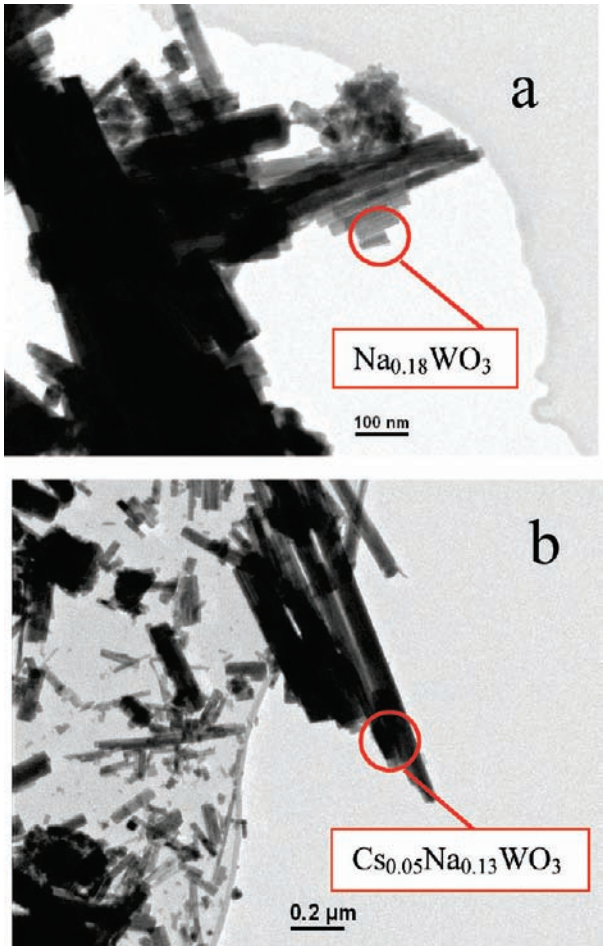

Figure 2. TEM and corresponding EDS analyses of (a) as-prepared acid-washed and (b) Cs-exchanged hexagonal tungsten bronze materials.

part of the HTB fibers. We have surmised that this was probably a result of excess NaCl in the preparation which remains even after extensive water washing. Washing with > 1 M HNO_3 was required to remove most of this excess Na^+ and much of the exchangeable Na^+ in the tunnels to leave a small amount of Na^+ that could not be removed regardless of the acid strength used (see part 1). During the Cs^+ ion exchange process in 1 M HNO_3, most of this excess Na^+ was removed. Since only the sodium in the tunnels was expected to affect the low-temperature transformation, no further attempts were made to remove sodium.

High-resolution ^{23}Na and ^{133}Cs magic-angle-spinning (MAS) NMR data were acquired at ambient temperatures on a Bruker MSL-400 spectrometer (B_0 = 9.4 T) operating at the ^{23}Na and ^{133}Cs frequencies of 105.81 and 52.50 MHz, respectively. All one-dimensional data were acquired with single pulses (Bloch decay) using a Bruker 4 mm double-air-bearing probe from which typical MAS frequencies of ∼15 kHz were implemented. For quantitative estimates of the central transition intensities to be made, the quadrupolar nature of the ^{23}Na (I = 3/2) and ^{133}Cs (I = 7/2) nuclei necessitated that flip angles be close to the condition[21,22]

$$(I + 1/2)\omega_{rf} t_p \leq \pi/6$$

Here, ω_{rf} is the radiofrequency and t_p is the pulse time.

For the ^{23}Na MAS NMR measurements, nonselective $\pi/2$ pulse times of 4.0 μs were measured in a 1.0 M NaCl solution, from which selective pulse times of 0.6 μs were employed for data acquisition on all solid samples. Relaxation delays of 3 s were typically used; however, the quantification and speciation of these data obtained with shorter recycle delays were verified with experiments which had delays extending to 30 s. All ^{23}Na chemical shifts were referenced to 1.0 M NaCl, which was set to δ 0.0 ppm. The ^{133}Cs MAS NMR pulse conditions were calibrated on a 1.0 M CsCl solution, where a nonselective $\pi/2$ pulse time of 6 μs was measured, from which selective pulse times of 0.6 μs were employed for data acquisition on all solid samples. Typical relaxation delays were 3 s; however, checks for abnormally long T1s were undertaken, with recycle delays of up to 60 s being implemented. All ^{133}Cs chemical shifts were referenced to 1 M CsCl, which was set to δ 0.0 ppm. All ^{23}Na and ^{133}Cs shifts are reported as center-of-gravity measurements and remain uncorrected for second-order quadrupolar effects unless specifically reported as isotropic chemical shift values δ_{iso} obtained from simulation or graphical methods.

^{23}Na two-dimensional multiple-quantum magic-angle-spinning (2D MQ-MAS) NMR studies[23−26] were undertaken at magnetic field strengths of B_0 = 8.45 and 14.1 T using Varian/Chemagnetics Infinity-360 and Infinity-600 spectrometers, respectively. At B_0 = 8.45 T (95.25 MHz), an amplitude-modulated triple-quantum (3Q) MAS NMR experiment[23,27] was used, which provided high-resolution hyper-complex 2D spectra whose indirectly detected (F1) dimensions have sign discrimination and are free from the second-order quadrupolar broadening exhibited by the central transition of the spin I = 3/2 ^{23}Na isotope. These measurements were achieved using a Bruker 4 mm probe and MAS rates of ∼8−10 kHz. In these experiments, 5.5 μs 3Q excitation pulses and 2.5 μs 3Q conversion pulses were utilized with RF field strengths of B_1 = 110 kHz, in conjunction with reduced-power (B_1 = 16 kHz) Z-filter pulses of 9 μs duration. Typical relaxation delays were 1 s, and each experiment took approximately 24 h. At 14.1 T (158.83 MHz), a phase-modulated split-t1 3Q MAS sequence[23] was implemented using a Varian 3.2 mm T3 probe and MAS rates of ∼10 kHz. For these experiments, 3.2 μs excitation pulses (B_1 = 155 kHz) and 10.0 μs echo pulses (B_1 = 30 kHz) were used. Maximum strength (B_1 = 155 kHz), single-period, sine-modulated 3Q conversion pulses of 4.0 μs periods were used to reduce the intensity lost by large C_Q lineshapes in the 3Q MQ-MAS NMR data. The echo times were 1.2 ms, relaxation delays were 2 s, and each experiment took approximately 24 h.

Samples for NMR analysis were dehydrated at various temperatures in a conventional laboratory oven and were transferred directly from the oven to a nitrogen-filled glovebox in which the H_2O and O_2 contents were < 1 ppm. Under these glovebox conditions, all samples were transferred into sealed polyethylene bottles. These bottles were stored under these anhydrous and reducing conditions until the

(21) Lippmaa, E.; Samoson, A.; Magi, M. *J. Am. Chem. Soc.* **1986**, *108*, 1730.
(22) Smith, M. E. *Appl. Magn. Reson.* **1993**, *4*, 1.
(23) Brown, S. P.; Wimperis, S. *J. Magn. Reson.* **1997**, *128*, 42.
(24) Fernandez, C.; Amoureux, J. P. *Chem. Phys. Lett.* **1995**, *242*, 449.
(25) Medek, A.; Harwood, J. S.; Frydman, L. *J. Am. Chem. Soc.* **1995**, *117*, 12779.
(26) Frydman, L.; Harwood, J. S. *J. Am. Chem. Soc.* **1995**, *117*, 5367.
(27) Amoureux, J. P.; Fernandez, C.; Steuernagel, S. *J. Magn. Reson. A* **1996**, *123*, 116.

subsequent transferal of each sample into airtight NMR rotors was performed, which was similarly undertaken under these controlled glovebox conditions.

Diffuse Reflectance Fourier Transform Infrared (DRIFT) spectra of the phases were recorded on undiluted materials in the range 400−4000 cm^{-1} with a Nicolet Nexus 8700 FT-IR spectrometer (Thermo Electron) employing a liquid-nitrogen-cooled HgCdTe detector. Samples were loaded into a platinum crucible and placed in a Spectra Tech Collector II DRIFT accessory equipped with a variable-temperature cell with KBr windows. Single-beam spectra at ambient and elevated temperatures (50−500 °C; 50 °C increments) were typically obtained at a resolution of 4 cm^{-1} and by averaging 256 scans. Kebulka−Munk transformations for the single-beam data were obtained using the single-beam spectrum of an optical mirror as the background. Decomposition of the Kebulka−Munk spectra were undertaken using the GRAMS/AI (version 8.0) software suite.

3. Results and Discussion

3.1. Thermal Transformations in Air: Na−W−HTB. Laboratory XRD powder patterns of as-prepared Na−W−HTB heated statically in the air at 70−450 °C are shown in Figure 3. A halving of the line width occurred as the temperature increased from 70 to 100 °C, and then little further change was observed up to 400 °C. At temperatures exceeding 400 °C, new reflections began to be observed in the pattern (Figure 3f), in particular around 10.8 and 21.8° 2θ, indicating the beginning of a phase transformation. Rietveld analyses of the patterns recorded after calcination in the range 70−400 °C indicated a progressive (almost linear) decrease in the unit cell volume (Figure 4a). Rehydration of the heated samples by reimmersion in water, filtering, and drying resulted in a partial restoration of unit cell volume, so that it appears that the dehydration process is only partially reversible up to 400 °C (Figure 4a). Heating to between 400 and 600 °C (not shown) resulted in the appearance of reflections characteristic of monoclinic WO_3, with no significant change in line width, which suggested that no significant crystallite growth occurred over this temperature range. Further heating to temperatures >700 °C facilitated the formation of a $Na_2W_4O_{13}$ phase, which was concomitant with WO_3 formation, thus representing the complete irreversible disproportionation of the Na−W−HTB phase.

Thermogravimetric Analysis − Differential Thermal Analysis (TGA-DTA) of the Na−W−HTB phase showed a progressive weight loss of 4.6% from ambient temperature to about 300 °C (Figure 4b). This corresponded to a total loss of 0.63 molecules of water per formula unit or about four molecules of water per sodium ion. Two weak endothermic peaks were observed at 94 and 239 °C, and these were probably due to the elimination of surface and intracrystalline water and correspond to weak inflections in the weight loss curves at these points. It is estimated that surface water accounted for about 1% weight loss, while the remaining 3.6% weight loss was due to intracrystalline water, which translates to three water molecules per sodium ion. The exothermic peak at about 513 °C is characteristic of a phase transition, and since this peak was observed at about the same

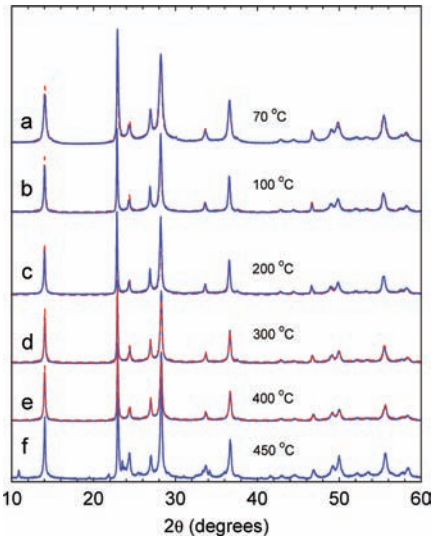

Figure 3. Experimental XRD patterns (solid lines) and associated Rietveld refinements (dashed lines) of Na−W−HTB heated in the air to various temperatures in the range 70−450 °C and examined at room temperature.

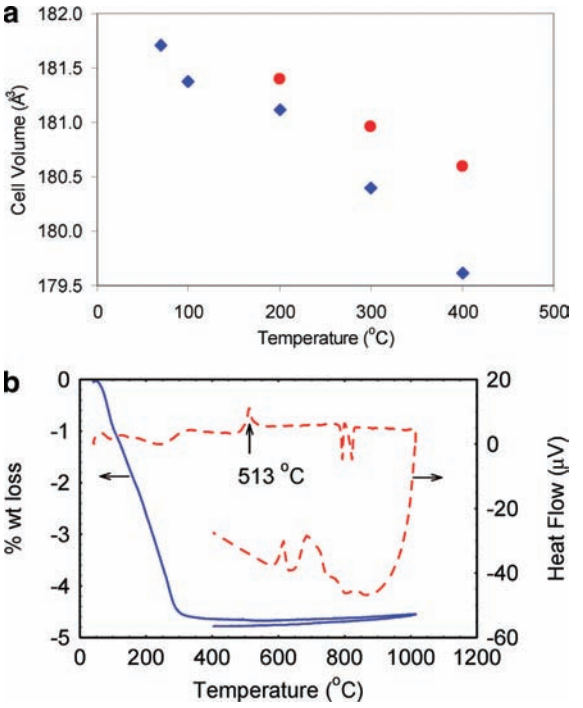

Figure 4. (a) Variation in unit cell volume as a function of heating temperature in the air for the Na−W−HTB before (◆) and after rehydration (●) and (b) TGA (—) and DTA (—) traces of Na−W−HTB.

temperature that WO_3 was first observed in the XRD pattern, we have ascribed this transition to the crystallization of WO_3. At 794 and 822 °C, two additional endothermic events were observed which are presumably due to the transformation from the hexagonal bronze structure to the WO_3 and $Na_2W_4O_{13}$ structures before the onset of melting.

The results of the thermogravimetric analysis−differential thermal analysis (TGA-DTA) are supported by variable-temperature DRIFT studies of the Na−W−HTB over the temperature range 35−300 °C (Figure 5). In the regions characteristic of O−H stretching

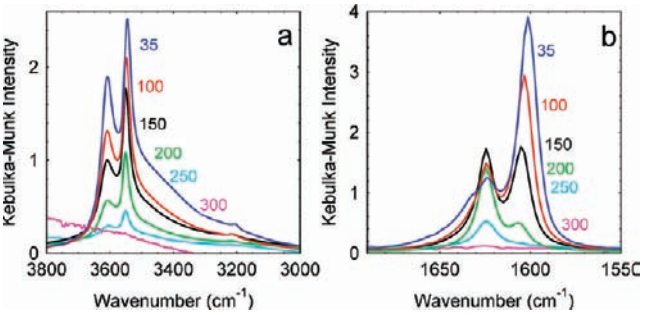

Figure 5. DRIFT spectra of Na−W−HTB heating over the range 35−300 °C in (a) the O−H stretching region (3800−3000 cm^{-1}) and (b) the H_2O bending region (1690−1550 cm^{-1}). The spectra were taken from 35 and 100 °C to 300 °C in increments of 50 °C and are shown in order of decreasing intensity.

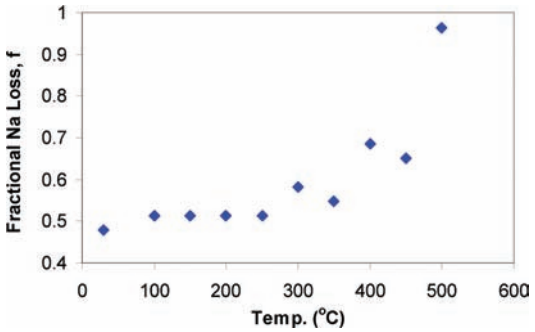

Figure 6. Fractional loss of Na from the Na−W−HTB phases heated in the air to increasing temperatures after contacting with 0.10 M HNO_3 at 140 °C for 4 days.

(3800−3000 cm^{-1}) and H_2O bending (1700−1550 cm^{-1}), there were observed three inter-related water species: (1) a loosely bound H-bonded water (broad band ~1650−1620 cm^{-1}) which was readily lost during the initial stages of heating, (2) a coordinated water that experienced a degree of H-bonding (1625 cm^{-1}) and that was lost on heating above 250 °C, and (3) coordinated water that experienced much less H-bonding (1603 cm^{-1}) and as such was lost entirely by 200 °C.

The leachability of tunnel Na^+ cations in Na−W−HTB phases heated to various temperatures in the range 70−500 °C was explored by contacting the samples with 0.1 M HNO_3 at 140 °C for a period of 4 days in sealed autoclaves. The fractions of Na^+ released to the aqueous phase from the calcined HTB samples are plotted in Figure 6 and indicate a gradual increase in fractional Na^+ loss up to 400 °C, then an abrupt further increase as for the phase heated to 500 °C. Thus, even though the unit cell volume was observed to shrink between 70 and 400 °C, Na^+ became more easily extracted from the tunnels, especially after heating at temperatures greater than 250 °C. The greatest level of Na^+ extraction occurred after the crystallization of WO_3 at about 500 °C and strongly suggests that the Na-rich phase resulting from the disproportionation of the Na−W−HTB phase is significantly more susceptible to leaching under these conditions.

3.2. Thermal Transformation in Air: Cs−W−HTB. Antithetically to the thermally treated Na−W−HTB phases, the leachability of Cs^+ from Cs−W−HTB phases thermally treated at comparable temperatures resulted in a dramatic decrease in the fraction of Cs^+ released from the solid to the aqueous phase once the calcination

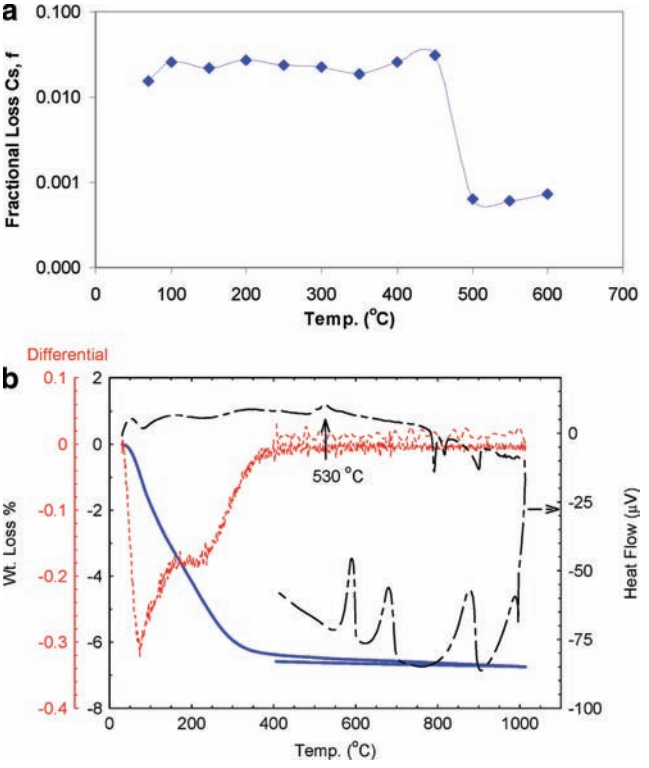

Figure 7. (a) Fractional loss of Cs^+ from the Cs−W−HTB phase as a function of calcination temperature (leaching conducted in 0.1 M HNO_3) and (b) thermal analysis traces of Cs−W−HTB phase. (—) TGA, (—) differential TGA, and (− - −) DTA.

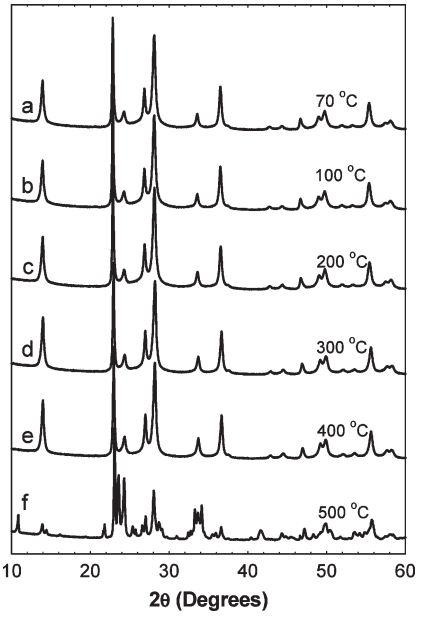

Figure 8. Experimental XRD patterns of Cs−W−HTB heated at 70−500 °C.

temperature reached about 450 °C (Figure 7a). As was the case for the Na−W−HTB phase, an exothermic peak was observed in the DTA trace at about 500 °C (see arrow Figure 7b). Heating at temperatures up to about 400 °C resulted in essentially no increase in the line width of HTB reflections in the XRD pattern (Figure 8), suggesting no increase in crystallite size up to this temperature. Cell volume contraction occurred at all heating temperatures

up to the temperature at which WO_3 was observed (500 °C) and then remained approximately constant up to about 600 °C. Cell volume determinations above this temperature became less precise as the proportion of WO_3 increased, and additional phases also appeared in the patterns. The exothermic peak in the DTA trace therefore once again coincided with the first appearance of WO_3 in the XRD pattern (Figure 8f).

The results of the variable-temperature DRIFT studies of the Cs−W−HTB over a comparable temperature range (Figure 9) are similar to those previously observed for the Na−W−HTB phase (Figure 7) with some subtle differences. Whereas in the Na−W−HTB sample three bands attributable to water bending from adsorbed water probably involved in H-bonding could be resolved, for the Cs−W−HTB sample at least four bands could be discerned in the 1590−1640 cm^{-1} range. The two intense water deformation bands at 1603 and 1625 cm^{-1} were clearly resolved as for the Na−W−HTB sample. However, for the Cs−W−HTB sample, a further two bands are observed as shoulders at 1630 and 1650 cm^{-1}. As judged by both the intense and well-resolved water deformation bands (1603 and 1625 cm^{-1}) and O−H stretching bands (3630 and 3545 cm^{-1}), there was significant retardation in the temperature at which this water was lost (i.e., the expulsion of water from the HTB tunnels). We suggest that this retardation could be due to cesium partially blocking the tunnels and not allowing water to be expelled from the tunnel sites.

3.3. Thermal Transformations in Vacuum: Na−W−HTB. For comparison with the samples heated in the air, heating was also conducted within the vacuum chamber of a high-resolution Debye−Scherrer synchrotron diffractometer. Dynamic heating in a vacuum in a sense parallels static heating in the air since evolved gases are allowed to escape. However, vacuum heating can result in changes in the oxidation state of the framework tungsten, which can influence phase transformations. For the upward-temperature run of the Na−W−HTB phase under vacuum conditions, powder diffraction data were recorded from room temperature up to about 800 °C in increments of 25 °C. Selected experimental data sets together with refinements carried out using the model of Reis et al.[11] as a starting point are shown in Figure10a−g. The oxygen atom from intratunnel water (O3) located at (0, 0, 0.4) was initially included in the refinements of all of the data and its occupancy refined (Table 1). This is

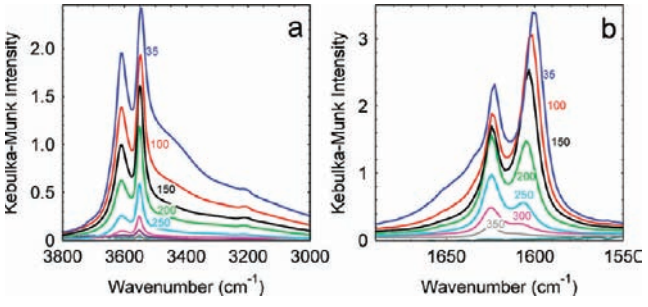

Figure 9. DRIFT spectra of Cs−W−HTB heating over the range 30−300 °C in (a) the O−H stretching region (3800−3000 cm^{-1}) and (b) the H_2O bending region (1690−1550 cm^{-1}). The spectra were taken from 35 and 100 °C to 450 °C in increments of 50 °C and are shown in order of decreasing intensity.

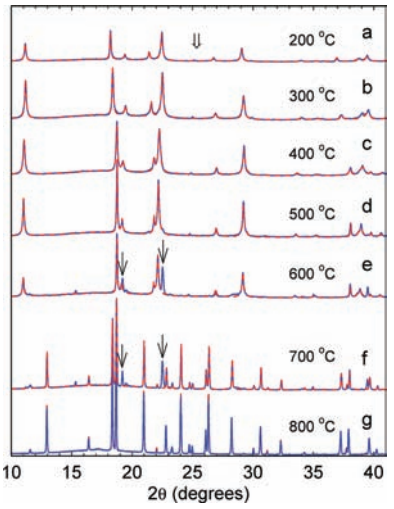

Figure 10. XRD patterns during dynamic heating of Na−W−HTB composition in a vacuum and associated Rietveld refinements (dashed lines). Arrows indicate new phase.

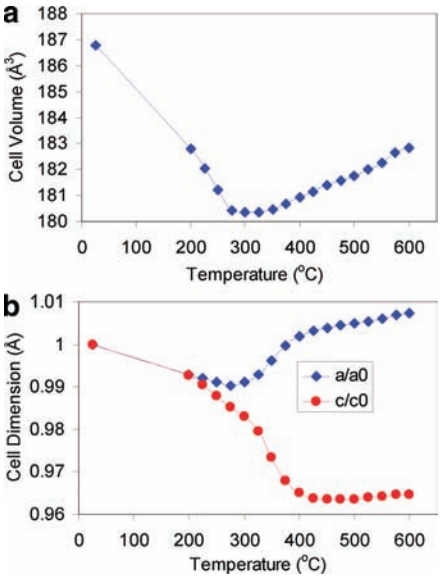

Figure 11. (a) Unit cell volume and (b) fractional changes in *a* and *c* dimensions of Na−W−HTB as a function of heating temperature in a vacuum: (◆) *a* dimension, (●) *c* dimension.

justified on the basis that the TGA shows that a very small amount of water may remain in the tunnels up to all but the highest temperatures investigated. In all cases, the refinement models represented good fits to each of the data sets, and only a very weak peak at about 25° 2θ (see ↓ symbol Figure 10a) was not accounted for. As the temperature was increased, the unit cell volume decreased quite significantly, reaching a plateau at about 300 °C, as can be seen from the plots of Figure 11a. Plots of the obtained cell dimensions along *a* and *c* (Figure 11b) showed that the reduction in cell volume was due to anisotropic changes along both of these directions with contraction along *c* and expansion along *a*. In the space group used, only O2 was not in a special position, and therefore the coordinates of this atom were allowed to vary during the refinement. It is apparent from the plot of the *x* and *y* coordinates of O2 that there was significant movement of this oxygen atom as a function of the

temperature. Therefore, it is concluded that the removal of water from the tunnels serves to expand the tunnel dimensions in the $a-b$ plane and contract along the c axis. This has the effect of bringing O2, which is part of the WO_6 octahedra defining the six-ring window, closer to the Na atom. However, some caution should be exercised in attaching excessive confidence in the positional coordinates for O2 obtained solely from refinement of X-ray data. As a check of these refinement values, we obtained variable-temperature neutron diffraction data for selected samples. Refinement of these data gave similar trends for the variations in the oxygen O2 position as a function of the temperature. Although not of primary concern to this study, above about 500 °C, additional lines were observed in the pattern that were not due to the HTB structure in *P*6/*mmm* (Figure 10d). At 600 °C, the pattern of the hexagonal bronze dominated, but additional reflections were observed at 15.3 and 22.5° 2θ (see ↓ Figure 10e). These lines could not be ascribed to any known sodium tungstate or tungsten oxide phase. The lines were also observed in the pattern recorded at 700 °C, but by 800 °C, only the pattern of a tetragonal tungsten bronze was observed.[28] Thus, an intermediate structure formed between 600 and 700 °C which coexisted first with the hexagonal tungsten bronze and then with the tetragonal bronze.

Unit cell volumes and *a*- and *c*-axis length variations extracted from the refinements of the XRD data obtained between 25 and 600 °C are plotted in Figure 11. The data show that the cell volume initially decreased dramatically by 3.5% between 25 and about 325 °C, and then increased through to 600 °C. The initial change corresponded to an initial contraction, or negative thermal expansion (NTE), along both the *a* and *c* axes (Figure 11b) of -2.36×10^{-5} and 6.88×10^{-5}, respectively. The contraction coincided principally with the loss of intracrystalline water, and we surmise that it was presumably caused by it. Unit cell shrinkage on the order of 0.64% has been observed from 42 to 147 °C for zeolites such as stillbite.[29−31] In the case of this zeolite, the shrinkage occurred as water was eliminated, and a phase transition from the monoclinic to orthorhombic structure was observed at 147 °C. At 600 °C, the cell volume was the same as at 200 °C, and therefore no net change in volume occurred over the temperature range investigated. However, above this temperature, additional water was expelled, and the structure continued to shrink and then collapse.

In the 325−425 °C temperature range, an upturn in cell volume with a net expansion of about 0.55% occurred. Examination of Figure 11b shows that this change was due to a positive thermal expansion along the *a*-axis ($\alpha = 8.82 \times 10^{-5}$) but a continued negative expansion along the *c*-axis ($\alpha = -1.31 \times 10^{-5}$). Above about 450 °C, the cell volume continued to increase linearly due to expansion along both the *a*- and *c*- axes. From the refinement data, it is clear that the hexagonal structure of *P*6/*mmm* remained intact over the 30−600 °C temperature range but that shrinkage of the structure does not occur uniformly as water was expelled.

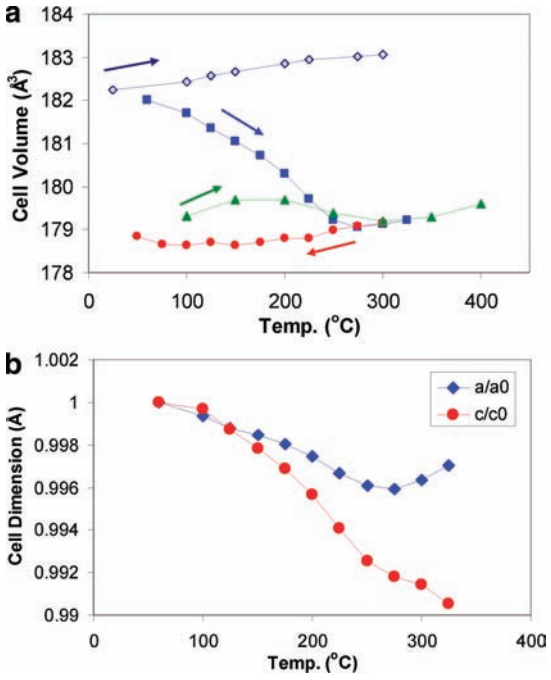

Figure 12. (a) Unit cell volume and (b) fractional changes in *a* and *c* dimensions of Na−W−HTB as a function of heating temperature in a vacuum. In a, the data markers are as follows: (■) first up-temperature run, (●) first down-temperature run, (▲) second up-temperature run, and (◇) single up-temperature run after heating in a sealed capillary.

Although the unit cell contraction in the 30−400 °C regime coincided with water loss, this could be coincidental. Therefore, to establish the origins of the cell volume contraction as a function of temperature in the low-temperature regime (30−300 °C), a second heating run was performed over this range only using an alternative Na−W−HTB sample with cycling. The results of these experiments are shown in Figure 12. For these data, the initial cell volume at 25 °C was somewhat lower than in the data of Figure 11, due to a difference in the initial state of hydration of the two specimens. Heating from 30 °C resulted in a comparable (%) unit cell contraction to 400 °C, as observed previously (■). Hence, it is believed that the negative thermal expansion is a general property of the sodium-containing HTB lattice. Subsequent cooling from this temperature (●) resulted in a further slight reduction in cell volume, while reheating from this temperature to about 200 °C (▲) afforded a slight increase in the measured cell volume. Interestingly, between about 200 and 300 °C of this secondary heating run, an additional reduction in cell volume was observed, and this was finally followed by re-expansion. Given the accuracy with which relative unit cell parameters are determined, it seems probable that the subtle contraction in the 200−300 °C temperature range was real.

3.4. Thermal Transformations in Vacuum: Cs−W−HTB. Vacuum heating of the Cs−W−HTB phase did not give rise to the crystallization of other phases at least up to 600 °C, as was observed for the Na variant (see Figure 7e−g). Presumably, this has to do with the stability that is conferred by the larger Cs^+ cations, which do not easily permit any kind of reconstructive phase transition. The thermally induced variations in cell parameters observed for this sample in a vacuum (Figure 13) followed similar trends to those observed for the Na−W−HTB

(28) Garcia-Ruiz, A.; Bokhimi, X. *Physica C* **1992**, *204*, 79.
(29) Alberti, A.; Vezzalini, G. *Proc. Int. Zeolite Conf., 6th*; Butterworths: London, **1984**; pp 834−41.
(30) Alberti, A.; Quartieri, S.; Vezzalini, G. *Eur. J. Mineral.* **1996**, *8*, 1273.
(31) Alberti, A.; Quartieri, S.; Vezzalini, G. *Stud. Surf. Sci. Catal.* **1994**, *84*, 637.

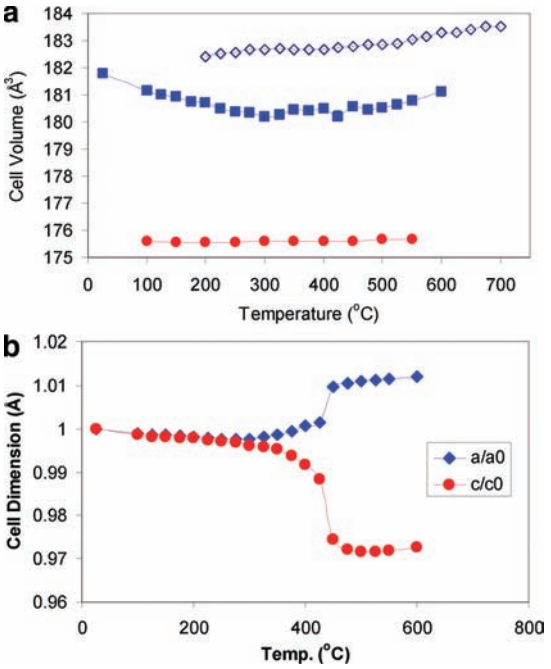

Figure 13. (a) Variation in unit cell volume and (b) fractional changes in *a* and *c* dimensions for Cs−W−HTB as a function of heating temperature in a vacuum. In a, the data markers are as follows: (■) up-temperature, (●) down-temperature, (◇) up-temperature in air in sealed capillary. Smoothed lines through the data points serve only as a guide to the eye.

phase, with the net thermal contraction along the *c*-axis being much greater than the net expansion along the *a*-axis. That is, an initial reduction in cell volume was observed between 300 and 400 °C and then a re-expansion. However, the contraction observed from room temperature to 325 °C was only on the order of 0.9%, not the 3.5% observed for the Na−W−HTB phase. We presume that this is due to the fact that the larger Cs^+ cation simply prevents any closer approach of the O2 atoms defining the window sites toward the Cs^+ site. In the 25−300 °C temperature range, both the *a*- and *c*-dimensions decreased slightly. However, as the sample became fully dehydrated (by about 300 °C), both the *a*- and *c*-dimensions began to trend in opposite directions. From about 300 to 600 °C, the decrease in *c* exceeded the increase in *a* so that only a relatively small net increase in cell volume was observed. It is extremely interesting to note, however, that regardless of these relative changes, the significant shrinkage along the tunnel axis has the effect of contracting the Cs−O2 bond length as found for Na−W−HTB. This is presumably due to the fact that there is a net thermal contraction of cell volume over the entire range 25−600 °C corresponding to a net large NTE along the *c*-direction of -47.6×10^{-6} K^{-1}. Such a value is extremely large when compared to the NTE observed for other materials. In the temperature range 300−600 °C, where there was no water present in the structure, the NTE along the *c*-direction was even larger at -78.7×10^{-6} K^{-1}.

At an elevated temperature (600 °C), the diffractometer was opened so that air was admitted and oxidation of the sample could occur. As is evident from Figure 13, a significant reduction in cell volume occurred, decreasing from 181.109 Å at 600 °C to 175.671 Å (3% decrease) at 550 °C on the down-temperature run (●). The pattern of the Cs−W−HTB was preserved throughout the downward-temperature run, and no WO_3 was observed in the patterns. The trends observed for the upward-temperature run under vacuum conditions (initial volume contraction followed by re-expansion) and monitored by X-ray diffraction were reproduced during neutron diffraction experiments conducted under similar conditions. On this occasion, however, the diffractometer was not opened at 600 °C (experimental requirement), and no such immediate reduction in cell volume was observed on the down-temperature run. Baring some hysteresis, we surmise that the cell volume on the downward-temperature run would track that of the upward-temperature run. The variation in the Cs−O2 distance as a function of temperature, measured using the neutron diffraction data, is plotted in Figure 14. It can be seen that the changes in the cell dimensions of the Cs−W−HTB lattice are also accompanied by changes in the Cs−O2 distance in a similar manner to that observed for the Na−W−HTB phase.

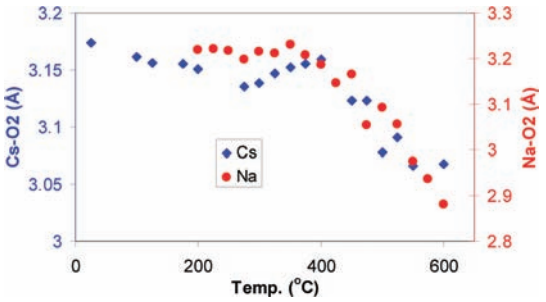

Figure 14. Variation in Cs−O2 (◆) and Na−O2 (●) distances as a function of temperature in a vacuum for Cs−W−HTB and Na−W−HTB, respectively.

3.5. ^{23}Na Solid-State NMR: Na−W−HTB. The ^{23}Na MAS NMR spectrum of as-synthesized Na−W−HTB at ambient temperatures is shown in Figure 15a with its associated spectral simulation. The Na speciation of the hydrated parent material was considered in detail in the preceding paper (Part 1) concerned with the room-temperature structure of the adsorbent phase. Briefly, the spectrum of the hydrated phase is comprised of three components, including a second-order quadrupolar broadened resonance characterized by a very large quadrupolar coupling constant (C_Q) of 5.2 MHz and an asymmetry parameter (η) of 0.0, which is observed at an isotropic chemical shift (δ_{iso}) of −4.0 ppm (species A), as well as two narrow, featureless ^{23}Na resonances at apparent shifts of $\delta \sim -6$ ppm (species B) and $\delta \sim -14$ ppm (species C). Species A was previously assigned to Na positioned within the hexagonal tunnel window position at the crystallographic (0, 0, 0) position and describes a strictly anhydrous hexagonal planar site (Scheme 1a). The high point symmetry of this position, which includes a C_6 axis of rotation, demands that $\eta = 0$, with the principal component (V_{zz}) of the ^{23}Na quadrupolar interaction tensor constrained (by symmetry) to be collinear with the unit cell *c*-axis. A C_Q of this magnitude is among the largest to be measured for any ^{23}Na system[32−35] and is

(32) Klosters, G.; Jansen, M. *Solid State Nucl. Magn. Reson.* **2000**, *16*, 279.
(33) Engelhardt, G.; Sieger, P.; Felsche, J. *Anal. Chim. Acta* **1993**, *283*, 967.
(34) Koller, H.; Engelhardt, G.; Kentgens, A. P. M.; Sauer, J. *J. Phys. Chem.* **1994**, *98*, 1544.
(35) Tijink, G. A. H.; Janssen, R.; Veeman, W. S. *J. Am. Chem. Soc.* **1987**, *109*, 7301.

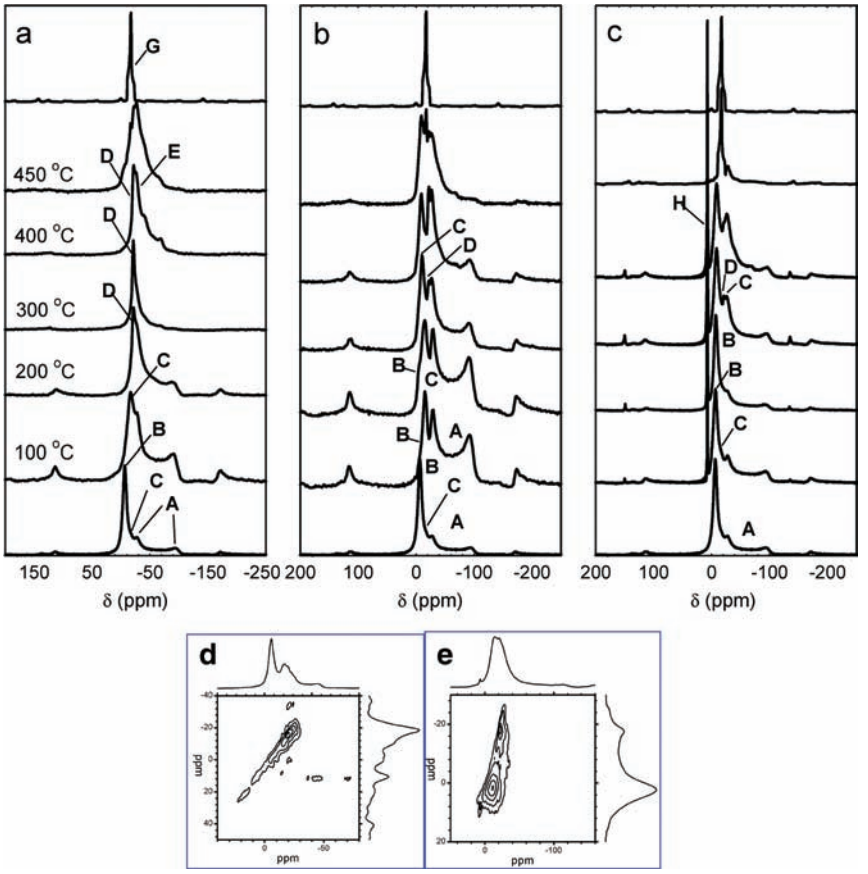

Figure 15. ^{23}Na MAS NMR spectra acquired at 400 MHz of Na−W−HTB (a) calcined at temperatures between 25 and 750 °C, (b) samples from part a after rehydration in ambient air for five days, and (c) samples from part a after rehydration in ambient air for three months. ^{23}Na multiple quantum (MQ) MAS NMR spectra of Na−W−HTB heated at 150 °C acquired at (d) 8.46 T and (e) 14.1 T. Dashed lines supperimposed on the experimental spectra of the 75 and 750 °C heated spectra are the simulations.

consistent with previously reported C_Q values describing pseudohexagonal planar[33,34] and hexagonal planar[35] Na sites. This measurement is also consistent with simplistic point charge calculations of quadrupole coupling constants undertaken by Koller et al., which demonstrated that sodium C_Q values on the order of ∼5−7 MHz are predicted for square-planar and hexagonal planar symmetries (Scheme 1a). Hence, the magnitude of C_Q and immediate coordination environment of this particular tunnel window position suggests that it be assigned to that of a completely anhydrous species.

The narrower species B and C ^{23}Na resonances (δ ∼−6 ppm and δ ∼−14 ppm, respectively) accompanying the quadrupolar dominated species A resonance at δ_{iso} −4.0 ppm are attributed to Na tunnel window positions in which some interaction with mobile tunnel water molecules occurs. The observed linewidths infer that a much reduced ^{23}Na quadrupole interaction exists at these positions; some degree of oxo-coordination with ligands (i.e., H_2O) along the tunnel direction (unit cell c axis) facilitates the observation of these resonances associated with reduced C_Q's. These ostensibly hydrated species B and C are tentatively assigned to di- and monohydrated sodium cations, respectively, and are schematically represented in the structural motifs of Scheme 1b,c. Such assignments are based solely on the proximity of these shifts to the hexaquo $Na(H_2O)_6^+$ shift reference at δ 0.0 ppm and the number of H_2O molecules constituting each hydration sphere; that is, increasing numbers of H_2O moieties forming an electrostatic contact with each Na^+ position produce a more electronegative ligand field and thus invoke a more downfield shift of the ^{23}Na resonance. Further evidence of the multiplicity of these additional hydrated sites is provided by the ^{23}Na 2D MQ-MAS data acquired at 8.45 and 14.1 T shown in Figure 15d and e, respectively. Both data sets exhibit contours that define two narrower resonances downfield from the broad anhydrous resonance, with each contour pitched at ∼60−70° to the axis (or along the QCS or chemical shift distribution axis),[24,36] indicating that the large degree of disorder exhibited by these species is dominated by chemical shift dispersion and not by distributions in the quadrupolar parameters. This suggests that the positional disorder of each hydrated Na moiety within the tunnel window site is minimal; however, there probably exists large distributions of Na−O(H_2) bond lengths characterizing these monohydrated and dihydrated variants given the overall mobility of the tunnel water. It can be observed in Figure 15d that the horizontal contour expected for the broad anhydrous tunnel window site (that exhibits characteristic short-range order) is not detected at 8.45 T due to the inefficiency of the RF pulses (B_1 = 110 kHz) in exciting to, and converting from, 3Q coherence pathways, with signal intensity being sacrificed as CQ increases. The smaller C_Q/P_Q ($P_Q = C_Q/2\sqrt{(1 + \eta 2/3)}$)

(36) Angeli, F.; Charpentier, T.; Faucon, P.; Petit, J. C. *J. Phys. Chem. B* **1999**, *103*, 10356.

Scheme 1. Possible Cartoon Schemes for Cation Siting Discussions

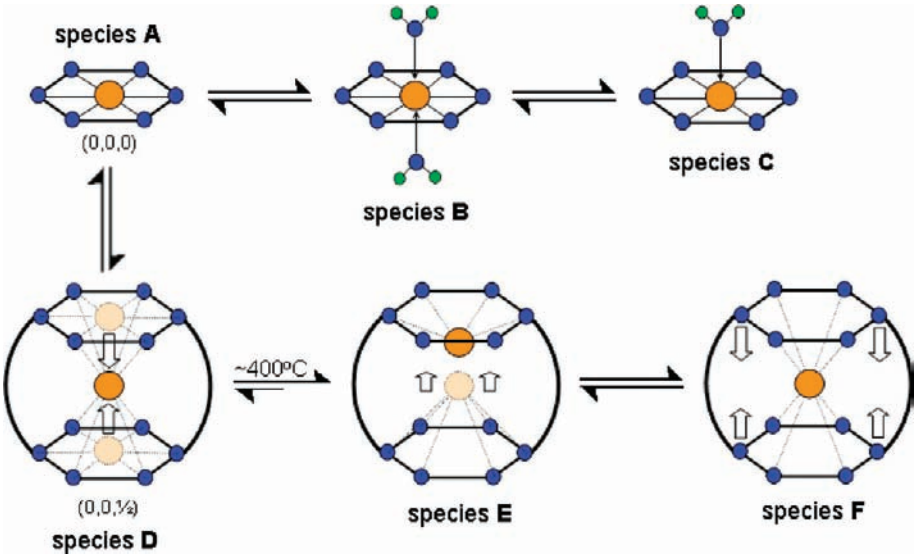

lineshapes therefore dominate these 8.45 T 2D data. However, the 14.1 T 2D data of Figure15e do exhibit low-intensity evidence of the horizontal contours expected for sites such as species A with short-range order, which is just visible above the noise. These features were detectable for a number of reasons: the line shape at 14.1 T is narrower; these 2D data were acquired with stronger RF pulses (B_1 = 155 kHz); the 3Q conversion pulses implemented were enhanced by modulations; and the signal was detected as an echo. The latter helps to prevent broad signals such as those from species A from being lost in probe dead times and beneath the resulting baseline distortions but requires an "echo" time period during which the ^{23}Na spins can lose coherence through T2 relaxation. This relaxation is the probable cause of the very different relative intensities observed for species B and C at 8.45 and 14.1 T.

Very pronounced and immediate changes to the as-synthesized Na speciation in the Na−W−HTB system are observed upon thermal transformation. In this dehydration/thermal transformation series, the ^{23}Na MAS NMR results of Figure 15a represent data from samples that were maintained in strictly anhydrous and reducing conditions. Mild heating to only 100 °C greatly simplifies this observed speciation with a large proportion of the assigned hydration effects being removed. The dominant downfield species B (dehydrated) Na position is now absent, and a reduced species C (monohydrate) presence is also evident, these being consistent with simple tunnel dehydration. Furthermore, the apparent position of the monohydrate species resonance has experienced a significant upfield shift from ∼−14 ppm to ∼+17.5 ppm, which is consistent with a longer Na−OH_2 interaction distance induced by increased mobility in the less-populated tunnels. Upon heating at 200 °C, it appears that the Na speciation has become unaffected by any residual tunnel hydration and that the onset of the first structural transformation influencing the Na speciation has now occurred. The Na speciation is now distributed between the original tunnel window position characterized by the broad δ_{iso} −4.0 ppm resonance and a new position represented by a very narrow resonance observed at an apparent shift of δ_{iso} ∼−21.2 ppm (species D). This new position is assigned to Na^+ cations that have migrated into the larger quasi-spherical cavity/void space subtended by the hexagonal window framework at each end and subsequently occupying the (0, 0, 1/2) position (see Scheme 1d). Such a position approximating spherical symmetry is consistent with a featureless resonance exhibiting a significantly reduced line width and is particularly characteristic of a very small quadrupole interaction at this new Na^+ position. The line shape of this resonance is completely Lorentzian in character, suggesting that this position is highly ordered, thus contrasting with the remaining Na speciation in this system, which exhibits a dominant Gaussian contribution primarily induced through the disorder associated with H_2O interactions. An additional upfield shift from ∼−17.5 ppm to ∼−21.2 ppm corroborates this observation, suggesting that no further Na−OH_2 interplay is experienced and that all Na tunnel speciation is essentially anhydrous. These observations are somewhat at odds with the DRIFT data of Figures 5 and 9 that report that the Na−W−HTB system remains partially hydrated at this temperature; however, this may be demonstrating that the tunnel rearrangement induced at this temperature could also be forcing the residual H_2O content into pocketed or regionalized occlusions which do not reflect a distribution throughout the tunnel confines. Further heating to 300 °C indicates that the Na−W−HTB system has entirely undergone this transformation with all Na^+ tunnel species now residing in the larger cavity voids, as evidenced by the sole remaining species D resonance, thus coinciding with the DRIFT data that suggest that the structure is now completely dehydrated, and the XRD data of Figures 11 and 12 that indicate a minimum in the unit cell volume. Further thermal transformation at 400 °C shows that additional Na species are introduced with a second-order quadrupole broadened resonance at δ_{iso} −29.0 ppm (C_Q = 3.45 MHz, η = 0.0) (species E) and another narrow featureless resonance observed at δ ∼−27 ppm (species F) concomitantly observed with species D. The

marked divergence in the unit cell *a* and *c* dimensions reported in the XRD study (see Figures 11 and 12) at this temperature induces a "tetragonal" compression on the quasi-spherical cavities (see Scheme 1e), with the more distorted cavities being characterized by a second-order quadrupolar dominated resonance (species E), suggesting that a 6-fold axis of rotation is maintained. The featureless (but broadened) resonance at $\delta \sim -27$ ppm (species F) probably represents less distorted moieties which are a transitional state between the quasi-spherical cavity position described by species D and the new "tetragonally" compressed cavity species assigned to species E. Further thermal transformation to 450 °C and above marks the onset of a disproportionation resulting in the formation/separation of a more condensed $Na_2W_4O_{13}$ phase and WO_3. At a temperature of ~750 °C, the transformation of the Na-bearing component portion of this system to $Na_2W_4O_{13}$ appears complete, and the new Na species is characterized by a second-order quadrupolar broadened resonance at δ_{iso} −10.8 ppm (C_Q = 1.45 MHz and η = 0.88). The more condensed nature of this phase is highlighted by the very large downfield shift of these ^{23}Na resonances from $\delta > 20$ ppm at 400 °C to δ_{iso} −10.8 ppm at temperatures ≥ 500 °C, demonstrating a much increased Na−O interaction through the shortening of these bond distances.

From a close inspection of Figure 15b and c, it is observed that a large proportion of the thermally induced transformations at temperatures ≤ 400 °C are reversible. Upon exposure of these samples to atmospheric conditions and further study by ^{23}Na MAS NMR, a large reversal of the change to the Na tunnel positions is measured. Significant change is detected after 5 days of atmospheric exposure (see Figures 15b), and more complete reversal back to the original Na−W−HTB system is observed after ~2 months of similar exposure (see Figure 15c). A study of the 100 and 200 °C data after 5 days of exposure in Figure 15b clearly shows that dihydrated and monohydrated species (species B and C, respectively) initially identified in the as-synthesized sample have returned at apparent shifts coinciding with their original characterization (see Table 2). The downfield shifts back from >17 ppm to ~6 ppm (dihydrate) and ~14 ppm (monohydrate) clearly demonstrate an increased Na−O affinity through re-emerging H_2O content within the tunnels. The most spectacular reverse-transformation, shown in Figure 15b, is observed for the Na−W−HTB sample heated to 300 °C; from a system that had undergone a virtually complete transformation to Na being sited in the quasi-spherical cavities, its speciation is now dominated by the broad δ_{iso} −4.0 ppm resonance and its hydrated variants, indicating a nearly complete migration back to the tunnel window position. It is interesting to note that any transformations undertaken at ≥500 °C are completely irreversible (see Figures 15a−c), and some component of Na^+ inventory is prone to leakage from the tunnel confines upon heating or aging (see Figure 15c). The latter observation is indicated by the appearance of a very narrow resonance at δ_{iso} 7.2 ppm, which corresponds to solid NaCl (species H). As these systems are synthesized using low pH conditions in the presence of HCl, product washing leaves some residual Cl^- on the surface of the resultant crystallites. Upon aging and heating (either during the thermal transformation process or from the gentle frictional rotor heating experienced under MAS conditions,[37] H_2O and Na^+ appear to migrate from the tunnels, and subsequent dehydration on the crystallite surfaces leaves residual NaCl. Similar observations have been reported from the MAS NMR studies of zeolites.[38]

Table 2. Measured ^{23}Na NMR Parameters from the Data Presented in Figure 15 for the As-Synthesized, Dehydrated and Rehydrated Na−W−HTB Systems

temperature/state	species	δ_{iso} (ppm)	δ (ppm)	C_Q (MHz)	η
as-synthesized/room temperature	A	−4.2		5.20	0.0
	B		~6		
	C		~14		
100 °C dehydrated	A	−6.8		5.05	0.0
	C		~−18		
200 °C dehydrated	A	−6.8		5.05	0.0
	D	~−21.2			
300 °C dehydrated	D	~−21.2			
400 °C dehydrated	D	~−21.2			
	E	−29.0		3.45	0.0
	F		~−29??		
750 °C dehydrated	G	−10.8		1.45/0.88	0.88
100 °C rehydrated	A	−4.3		5.10	0.0
	B		~−6		
	C		~−15		
200 °C dehydrated	A	−4.3			
	B		~−6		
	C		~−15		
300 °C dehydrated	A	−4.3		5.10	0.0
	B		~−4		
	C		~−11		
	D	~−21.2			
400 °C dehydrated	A	−4.3		5.10	0.0
	B		~−4		
	C		~−10		
	D	~−21.2			

The long-term reverse transformation series of Figure 15c is more efficiently analyzed if the individual components are quantitatively evaluated and their corresponding ^{23}Na chemical shifts monitored as a function of the temperature. The subsequent simulation and deconvolution of all of the ^{23}Na MAS NMR data of Figure 16 are summarized in Figure 17. From Figure 17, it can be observed that (to within experimental error of each measurement and simulation) the quantitative sum of the narrower resonances attributed to the dihydrated and monohydrated species remains virtually unchanged throughout the room temperature to 400 °C temperature regime; this is mirrored by similar static behavior of the broad quadrupolar dominated resonance representing the anhydrous species A. Although the total hydrated component of the tunnel Na speciation remains constant, there is significant variation between the dihydrated and monohydrated moieties, with the dihydrated Na species appearing to be more favored at the lower temperatures; however, at 400 °C, the monohydrated species assumes dominance. This is consistent with the monotonic unit cell contraction observed (by XRD) over this temperature

(37) Van Gorkom, L. C. M.; Hook, J. M.; Logan, M. B.; Hanna, J. V.; Wasylishen, R. E. *Magn. Reson. Chem.* **1995**, *33*, 791.
(38) Seidel, A.; Tracht, U.; Boddenberg, B. *J. Phys. Chem.* **1996**, *100*, 15917.

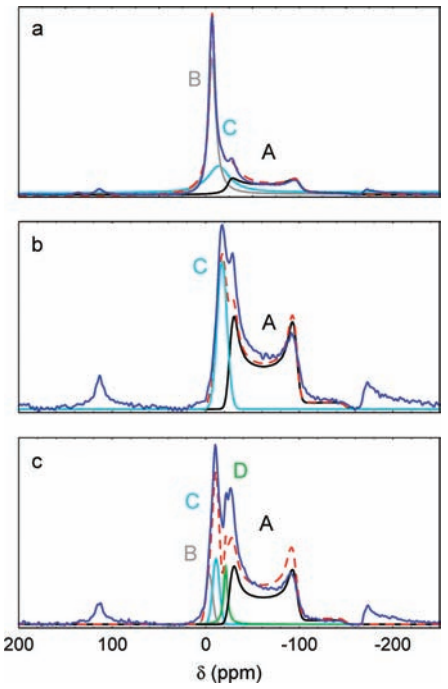

Figure 16. ^{23}Na MAS NMR spectra and simulations for Na−W−HTB (a) as-prepared, (b) dehydated at 100 °C, and (c) dehydrated at 300 °C and then rehydrated for five days: (—) experimental spectrum ,(—) sum of all components.

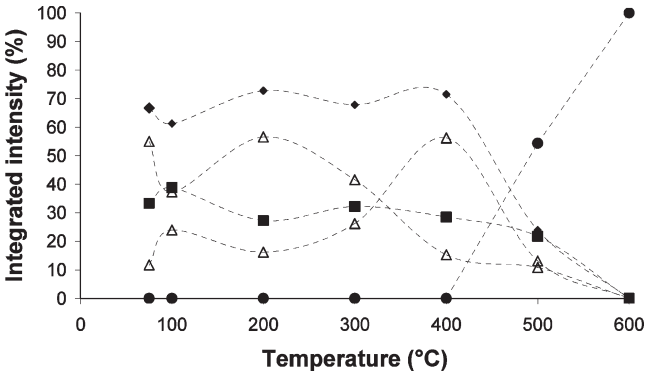

Figure 17. Intensity variation of ^{23}Na NMR species as a function of temperature extracted from simulations: (◆) disordered sum, (●) C_Q = 1.45 MHz, (■) C_Q = 5.2 MHz (species A), (△) two disordered species.

range facilitated predominately by shortening along the *c*-axis. Such a unit cell decrease introduces reduced tunnel volumes and thus prohibits more complete hydration spheres of the Na tunnel window positions from forming. This observation also supports the original assignments of the dehydrated and monohydrated tunnel window species, with the low-field ^{23}Na resonance being associated with the dehydrated variant. These ^{23}Na MAS NMR data suggest that the Na−W−HTB tunnel dehydration occurring via thermal transformation in the low-temperature regime is a highly dynamic and reversible process. It appears that water uptake in the tunnels occurs readily, and the equilibrium between the hydrated and anhydrous Na species is constantly re-established, albeit with modified proportions between hydrated variants being introduced.

3.6. ^{133}Cs Solid State NMR: Cs−W−HTB. The 400 MHz ^{133}Cs MAS NMR spectra of a HTB sample saturated with cesium which had been dried at 70 °C or heated between 100 and 500 °C are shown in Figure 18. Previous investigations by our group have demonstrated that the complex line shapes often observed for cesium-containing HTB frameworks generally result from the presence of multiple cesium environments and not second-order quadrupolar interactions.[15]

The progressive removal of water has varied effects on the isotropic chemical shift and relative intensity of the cesium species identified by the spectral decomposition. In the spectra of the sample dried at 70 °C, two principle components were observed at δ −33.35 and −63.26 ppm, with a minor component of minimal intensity at δ −40.93 ppm. Heating to 100 °C had little effect on the position and relative intensity of the two principle components. On raising the temperature to between 200 and 400 °C, a new resonance appeared at about −16 ppm, while the other two resonances were preserved, although their isotropic chemical shifts were shifted somewhat. This new component was centered ostensibly at the same chemical shift as the single species identified in the sample heated to 500 °C (δ −16.74 ppm). Hence, we attribute this resonance to cesium atoms which are devoid of water in their coordination sphere and sitting in the regular tunnel site indicated by crystallography (i.e., at position 0, 0, 0). The line width of the resonance suggests that the cesium experiences significant positional disorder. Slight variations in composition should also not be discounted. There is clearly no water in the coordination sphere of this Cs^+ species, which emphasizes that the other components of the lower-temperature spectra are cesium species of varying hydration. It is impossible to comment on the precise hydration number of cesium which each of these components represents, except to say that an increase in hydration number would be expected to increase the deshielding about the cesium nuclei and shift the associated resonance to a higher field. Importantly, the spectral decompositions indicate that at least three cesium species are present in Cs−W−HTB heated up to at least 400 °C. Thus, the

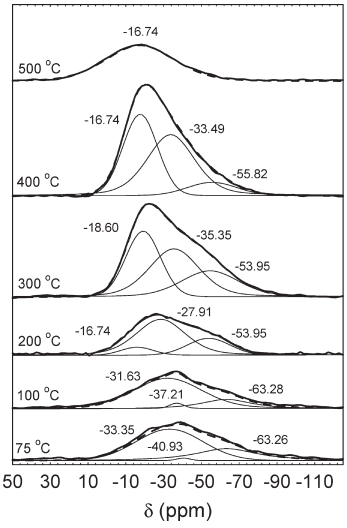

Figure 18. ^{133}Cs MAS NMR spectra acquired at 400 MHz of cesium-saturated HTB calcined at temperatures between 80 and 500 °C. Spectral decompositions are shown by the thick dashed lines with each of the components shown by thin lines.

number of unique Cs^+ environments is similar to that observed for Na^+. The complete expulsion of water from the Cs−W−HTB lattice is not complete until between 400 and 500 °C, as judged by TGA/DTA and variable-temperature DRIFT spectroscopy, and it is at this point that we believe that the locking in of Cs occurs (dramatic reduction in leachability).

In part 1 of this series, it was observed that the hydrated parent material could readily exchange a proportion of the initially present tunnel Na^+ species for a variety of cationic species. Particular emphasis in this and earlier studies of this material was placed on explaining the basis of Na^+ for Cs^+ and Na^+ for Sr^{2+} ion exchange selectivity of the HTB framework, since these cations are of interest in the pretreatment of radioactive nuclear waste. It was observed that not all of the Na^+ in the parent material was exchangeable and that even mild thermal treatment in the air at temperatures below 200 °C was sufficient to profoundly modify the ion-exchange properties of the HTB framework. In the case of Cs^+ ion exchange, the affinity of the framework, as measured through the distribution coefficient, seemed to increase after mild dehydration, reaching a maximum after about 150 °C dehydration and thereafter decreasing linearly. On the other hand, for Sr^{2+} ion exchange in the parent material, the distribution coefficient decreased linearly from room temperature. Such results begged an explanation, and therefore in the present study we have undertaken to glean an understanding of the dehydration dynamics of the HTB framework. The XRD data of this study have born out that mild dehydration is sufficient to drive water out of the unidimensional tunnels, resulting in anisotropic shrinkage of the tunnels. Measurable shrinkage was observed in the unit cell parameters even after dehydration at temperatures as low as 100 °C. This shrinkage was not easy to reverse, and even emersion in water seemed to only partially restore the tunnel dimensions of materials heated in the air. It is clear that, since the tunnel environment is very restrictive to start with, little change in dimensions can be tolerated before the impacts are seen in the properties of the materials.

Although the tunnel dimensions of both the Sr^{2+}- and Cs^+-exchanged variants underwent shrinkage (anisotropic unit cell contraction) on mild dehydration, there were differences in magnitude. For Sr−W−HTB, the changes were quite large, and a phase transition eventually occurred at around 500 °C. Shrinkage was less pronounced in the Cs−W HTB variant, and the HTB framework retained its integrity to much higher temperatures. Although the XRD results provided an averaged picture of a dynamic dehydration process, solid-state NMR afforded a cation selective view showing that there was considerable multiplicity in the environment of both the Na^+ and Cs^+ cations that was not suggested by the X-ray or neutron diffraction data. In the case of both Na^+ and Cs^+, at least three unique sites could be distinguished in the parent Na−W−HTB and Cs−W−HTB materials, respectively. For the former, this multiplicity was greatly reduced by 300 °C, while for the latter, it took dehydration to 500 °C to achieve a single Cs^+ environment. While the changes in unit cell dimensions showed a degree of reversibility below about 400 °C, at higher temperatures, this was effectively eliminated. After complete water removal in a vacuum at temperatures beyond 300 °C, unit cell expansion was only slight and driven mainly by expansion along the *a* direction while the *c* dimension remained essentially unchanged.

4. Conclusions

In this work, we have sought to furnish an understanding of the nature of low-temperature thermal transformations and dehydration dynamics of oxidized hydrothermally prepared hydrous HTB ion exchange materials. Thermal variations in unit cell dimensions are anisotropic, but there is a net thermal contraction on heating to temperatures in the range 25−600 °C. This irreversible contraction along the *c*-direction explains the locking in of Cs in the structure at even these low temperatures.

Although the general thermal transformations, namely, consistent net unit cell contraction, are similar for both the Na and Cs phases of the alkali-rich tungstate phases which are formed at around 500 °C, only in the case of Cs is the alkali element locked into the resultant phase. It is our conclusion that this probably is due to the size of cesium, the irreversible nature of the dehydration process prior to phase change, and the restrictive nature of the tunnels and redistribution of tunnel cations.

The fundamental understanding of the way that the Cs−W−HTB phase behaves during the early stages of calcinations (in air) affirms our previous studies, which suggested that durable HTB phase assemblages are accessible either in the presence or absence of alkali cations. In this case, the alkali cations are sodium, with the presence of H^+ also not being forgotten.

Another important aspect of the HTB system is that only 500 °C is required to drop fractional Cs losses below 0.0001, which is potentially extremely useful from a radioactive waste management perspective since it allows the same basic framework to be used first for selective extraction of target species and then their immobilization through the use of temperatures that are less than half of those required to prepare competing ceramic waste form materials such as Cs-hollandite.

Acknowledgment. The authors are indebted to Dr. C. J. Howard of ANSTO for useful discussions and invaluable assistance with acquisition of the neutron data. We are also grateful to Dr. Kim Finnie of ANSTO for assistance with the recording of the DRIFT spectra. The synchrotron measurements at the Australian National Beamline Facility were supported by the Australian Synchrotron Research Program, which is funded by the Commonwealth of Australia under the Major National Research Facilities program. We thank Dr. James Hester and Dr. Garry Foran for their assistance with these measurements.